THE ASTROPHYSICAL JOURNAL, 457:169–176, 1996 January 20

THE STEEP SOFT X-RAY SPECTRUM OF THE HIGHLY VARIABLE ACTIVE NUCLEUS IN MARKARIAN 478

H. L. MARSHALL[1] AND T. E. CARONE[2]
Eureka Scientific, Inc., 2452 Delmer Street, Suite 100, Oakland, CA 94602
J. MICHAEL SHULL
Center for Astrophysics and Space Astronomy, and Joint Institute for Laboratory Astrophysics, University of Colorado and National Institute of Standards and Technology, Campus Box 440, Boulder, CO 80309
M. A. MALKAN
UCLA, Department of Astronomy, Los Angeles, CA 90024
AND
M. ELVIS
Harvard-Smithsonian Center for Astrophysics, 60 Garden Street, Cambridge, MA 02138
Received 1994 December 28; accepted 1995 July 28

ABSTRACT

We present the first moderate-resolution spectrum of the soft X-ray excess in an active galactic nucleus. Mrk 478 was detected in the 70–100 Å spectral region using the *Extreme Ultraviolet Explorer* (*EUVE*) spectrometer. The spectrum shows no significant spectral features and is consistent with a very steep power law. The neutral hydrogen absorbing column is consistent with the Galactic value. The spectral slope is poorly determined if the absorbing column is allowed to vary; $\alpha = 27 \pm 9$ ($f_\nu \propto \nu^{-\alpha}$), and the best-fit column density (cm^{-2}) is $\log N_H = 20.6$. If the column density is fixed at the Galactic value, $\log N_H = 20.0$, then $\alpha = 4.70 \pm 0.65$.

The lack of emission lines and significant variability indicate that the soft X-ray continuum is *not* due to emission from a thin thermal plasma or a leaky neutral or warm absorber. There is marginal evidence that the spectrum hardens as it brightens, which is consistent with thermal variations rather than absorption changes. If this component is the Wien tail of a blackbody spectrum, then the temperature at the inner edge of the accretion disk must be of order 10^6 K. For an accretion disk model from Sun & Malkan (1989), we require a mass of $1.3 \times 10^8\ M_\odot$, an accretion rate of $0.3\ M_\odot\ yr^{-1}$, and a highly inclined disk, with $\cos i = 0.50$, in order to keep $L < L_{Edd}$.

Subject headings: galaxies: active — galaxies: individual (Markarian 478) — galaxies: nuclei — radiation mechanisms: nonthermal — ultraviolet: galaxies — X-rays: galaxies

1. INTRODUCTION

Studies have shown that many active galactic nuclei (AGNs) have spectral "excesses" that can more than compensate for the effects of galactic absorption (e.g., Branduardi-Raymont et al. 1985; Wilkes & Elvis 1987; Turner & Pounds 1989) when extrapolating harder X-ray spectra below the K edge of carbon (at 0.28 keV or 44 Å). These observations indicated that AGNs would be detectable in the extreme ultraviolet (EUV), as predicted by Marshall (1991). Indeed, the first EUV all-sky surveys (Pounds et al. 1993; Malina et al. 1994) show that AGNs are among the first several hundred brightest EUV sources in the short-wavelength band (shortward of 150 Å). Marshall et al. (1995) presented the EUVE all-sky survey results, in which 13 extragalactic point sources were detected.

In this paper, we present the first EUV or soft X-ray spectrum of Mrk 478. *ROSAT* observations indicate that this AGN has a steep X-ray spectrum ($\alpha = 2.5$; Gondhalekar et al. 1994), and the Galactic column density to the source was found to be consistent with the 21 cm Bell Lab value (Stark et al. 1992), $N(H\ I) = 1.2 \times 10^{20}\ cm^{-2}$, making this an unusually favorable source to observe with the EUVE spectrometer. These data can be used to test models of the soft X-ray excess by direct observation. Furthermore, variability of the broadband soft X-ray flux was monitored during the observation, which lasted for about a week.

2. OBSERVATIONS

The target for this observation, Mrk 478, was selected for spectroscopy because it was the brightest AGN in the *ROSAT* WFC survey (Pounds et al. 1993). It was detected by the WFC at a count rate of 0.052 count s^{-1} (Pounds et al. 1993). It was also detected using *EUVE* scanning telescopes during the all-sky survey gap "fill-in" at a rate of 0.0515 count s^{-1}, according to Marshall et al. (1995).

Mrk 478 was observed for 300,000 s from 1993 April 8 to 1993 April 18 with the *EUVE* spectrometer (Malina et al. 1994). The observation was divided into four time segments, alternating from on boresight, where the calibration is best determined, to 0°.3 off-axis. The off-axis observations were taken so that the spectrum is shifted in the dispersion direction on the detector in a direction such that the shorter wavelengths could be observed in the short-wavelength detector. Specifically, during on-axis observations, the shortest wavelength would be about 72 Å, near the edge of the detector. When the

[1] Please send reprint requests to hermanm@usa1.com or 5 Whipple Road, Lexington, MA 02173.
[2] Also Space Sciences Laboratory, University of California, Berkeley, CA 94720.

spectrometer is pointed 0°.3 off-axis, the edge of the detector corresponds to a wavelength of 64 Å.

There are other advantages to off-axis observations. Besides getting the opportunity to detect shorter wavelengths than with on-axis observations, the background is reduced considerably because it is dominated by geocoronal Lyα scattered within the telescope. This background increases toward the edge of the detector at the short-wavelength end. Shifting the detector moves the spectrum relative to the background, which is fixed in detector coordinates. Another advantage of shifting the spectrum is that the detector distortion decreases away from the detector rim. Finally, after the observations were obtained, we learned that the width of the spectrum in the imaging direction was slightly smaller than the on-boresight width so that the eventual signal-to-noise ratio would be higher.

2.1. *Spectrometer Observations*

The spectral data were reduced in three steps. First, all data were restricted to times when the detector (ADC) count rates were less than 50 counts s^{-1}. This step eliminated data dominated by the edge of the South Atlantic Anomaly and other high background periods. Second, the off-axis observations were combined and the spectra were extracted using the apall routine in IRAF.[3] The aperture was traced carefully to follow the curvature of the spectrum in detector coordinates, which is due to detector wavelength mapping distortions. The aperture was defined by determining the spectrum centroid in the imaging direction in 10 Å width bins shifted 5 Å at a time. A simple rectangular aperture was used to extract a spectrum from the on-axis portion of the observations because the on-axis data were better corrected for detector distortions using the updated *EUVE* calibration data (v.1.8). Background regions 30 pixels wide were chosen on either side of the spectrum. Larger width regions caused systematic overestimation of background at the short-wavelength end of the spectra due to the curvature of the scattered Lyα background. Finally, the two spectra were blocked into 1 Å bins, combined and then divided by the (interpolated) spectrometer effective area function. The spectrometer resolution is 160–200 in the 70–100 Å band, so there is only slight resolution loss in binning to 1 Å.

Before combining, we confirmed that the spectra taken on-axis were consistent with those taken off-axis because there is currently no independent calibration of the *EUVE* spectrometer's off-axis response. Preliminary reduction and analysis of on- and off-axis observation of the white dwarf HZ 43 indicate that the effective area of the short-wavelength spectrometer changes by less than 10% for all wavelengths from 70 to 100 Å as the boresight is offset by 0°.3 (Marshall & Dupuis 1995). Given the priminary nature of this result and the low signal of the data, we applied the same effective area function for the off-axis data as for the on-axis data. The two count rate spectra were combined by applying weights based on the uncertainties. At the edges of the detector, the bright rim causes significant background subtraction errors, so the data at the rim and beyond were ignored. Exposure losses due to "Primbsching"[4] and dead time were not corrected because the corrections are expected to be less than 5% (see Marshall 1995) for the ADC count rate selection used and are not significantly variable. The final spectrum is shown in Figure 1.

2.2. *Light Curve from the Deep Survey Detector*

The deep survey (DS) detector obtained a direct image of Mrk 478 at the same time as the spectrum was taken. A good detection of the source is measured for each orbit because the light is not dispersed, and the effective area is ~10 times higher than that of the short-wavelength spectrometer. The light curve obtained using the DS point spread function and a likelihood method (Marshall 1995) is shown in Figure 2*a*. The dashed vertical lines in the figure differentiate different pointing positions: the first and third are taken on-axis, and the remaining two periods were obtained off-axis.

After the observations were completed, it was determined that there is a small region of reduced gain and detector quantum efficiency near the center of the DS detector which was caused by a "scrubbing" effect during the observation of the very bright EUV source HZ 43. This dead spot causes a reduction in the observed count rate by at most a factor of 4 when the target is very near the telescope boresight (Sirk 1994). The magnitude of the deadspot and its size are well documented by Sirk, using observations of white dwarfs, which should not vary significantly. Sirk produced a map of the image intensity degradation as a function of location near the on-axis imaging location. He finds that the center of the dead spot is at a detector coordinate (1030, 1023) and the 50% correction region is about 30 pixels across. Sirk shows that corrections can be reliably applied if the distance of the image centroid from the dead spot center is greater than about 7 pixels while the corrections are only good to 25%–50% for smaller distances.

Although the on-axis data are affected by the dead spot, it is clear that the source is highly variable just by examining the off-axis observations. There is no dead spot of which we are aware at this off-axis angle, and the detector response is known to be constant to better than 3% on small scales, so we believe that these variations are intrinsic to the source. There are increases of a factor of 2 over timescales of about 0.5 day during both of the off-axis observations, and the average level of the count rate is significantly different.

The variations during the first on-axis observation are dramatic, larger than the off-axis variability, so it is worthwhile to attempt to correct for the deadspot. The source was 8–15 pixels and then 4.5–7.5 pixels from the dead spot center during the first two orbits after acquisition. Using corrections based on a map of the dead spot (Sirk 1994), we estimate the efficiency of the DS detector to be 0.8 and 0.7 for these two orbits, which should be good to about 15%. For all the remaining on-axis observations after these first two orbits, the source centroid was located within 4 detector pixels of the dead spot 95% of the time and within 2 pixels half the time. As pointed out by Sirk, the actual image location is highly uncertain when the image is this close to the center of the dead spot because the shape of the point spread function is sensitive to the exact location of the image. Since the measured positions are fairly stable, we suggest that the dead spot efficiency should also be stable. Using the dead spot map, we would obtain a value of 0.25 to 0.4 when the source is less than 4 pixels from the dead spot center, so a value of 0.33 appears reasonable. Examining the transitions between the off-axis and on-axis pointings,

[3] IRAF is supplied and maintained by NOAO.

[4] This term refers to the way telemetry is allocated dynamically on the spacecraft. If the detector produces fewer than $1/N$ of the total allowed telemetry spaces (where N is the number of detectors), then all the events are guaranteed to be downlinked. The algorithm is named for its author, Henry Primbsch.

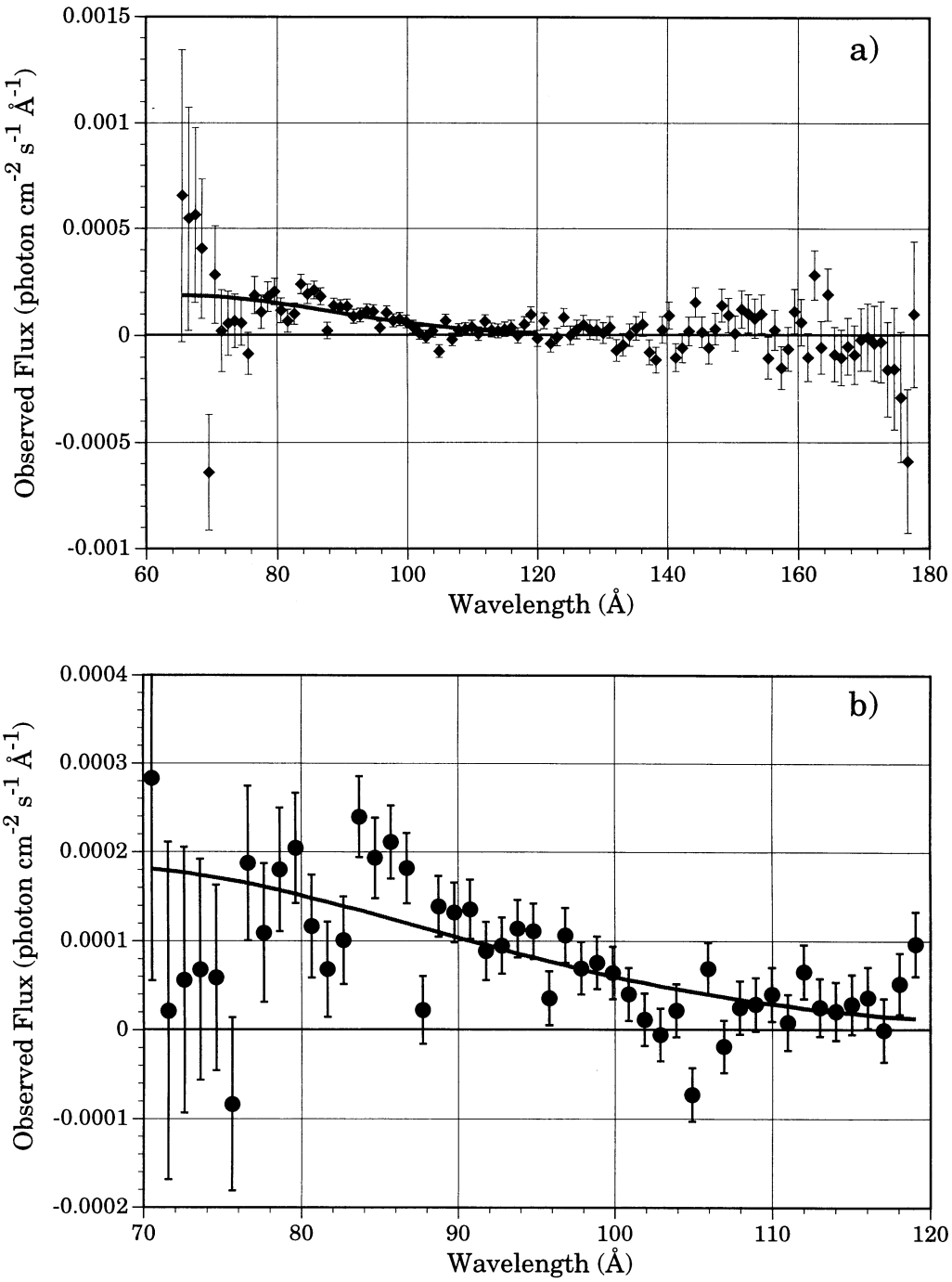

FIG. 1.—Soft X-ray spectrum of Mrk 478 taken with *EUVE*. *Filled circles:* Data from *EUVE* with derived statistical uncertainties. *Gray line:* best-fit power-law model ($f_\nu \propto \nu^{-\alpha}$) with $\alpha = 4.2$ and N_H fixed to the Galactic value of 10^{20} cm^{-2}. (*a*) The entire spectrum from 65 Å to 177 Å, which shows no detections longward of 120 Å. (*b*) Spectrum expanded to show detail in the region of good detections. The model has a formally poor χ^2 value, which results from a few small spectral deviations rather than a systematic trend.

however, we note that there is a jump in the observed (uncorrected) count rate by only a factor of 2 in the apparent count rate at each of the three transitions. Therefore, we assume an efficiency value of 0.50 for all remaining on-axis data to produce the solid points in Figure 2*a*, which provide more smooth transitions between the on-axis and off-axis observations. Given the uncertainty in the correction factor and the stability of the pointing direction, there probably remains a 20%–30% systematic uncertainty on the individual on-axis measurements. Unfortunately, this creates a corresponding 10%–15% systematic uncertainty on the average DS count rate for the entire observation, which is 0.099 count s^{-1}.

A light curve (Fig. 2*b*) was derived from the short-wavelength (SW) spectrometer data by simply summing data in a rectangular aperture spanning the 75–85 Å region and subtracting the appropriate background. The statistics are

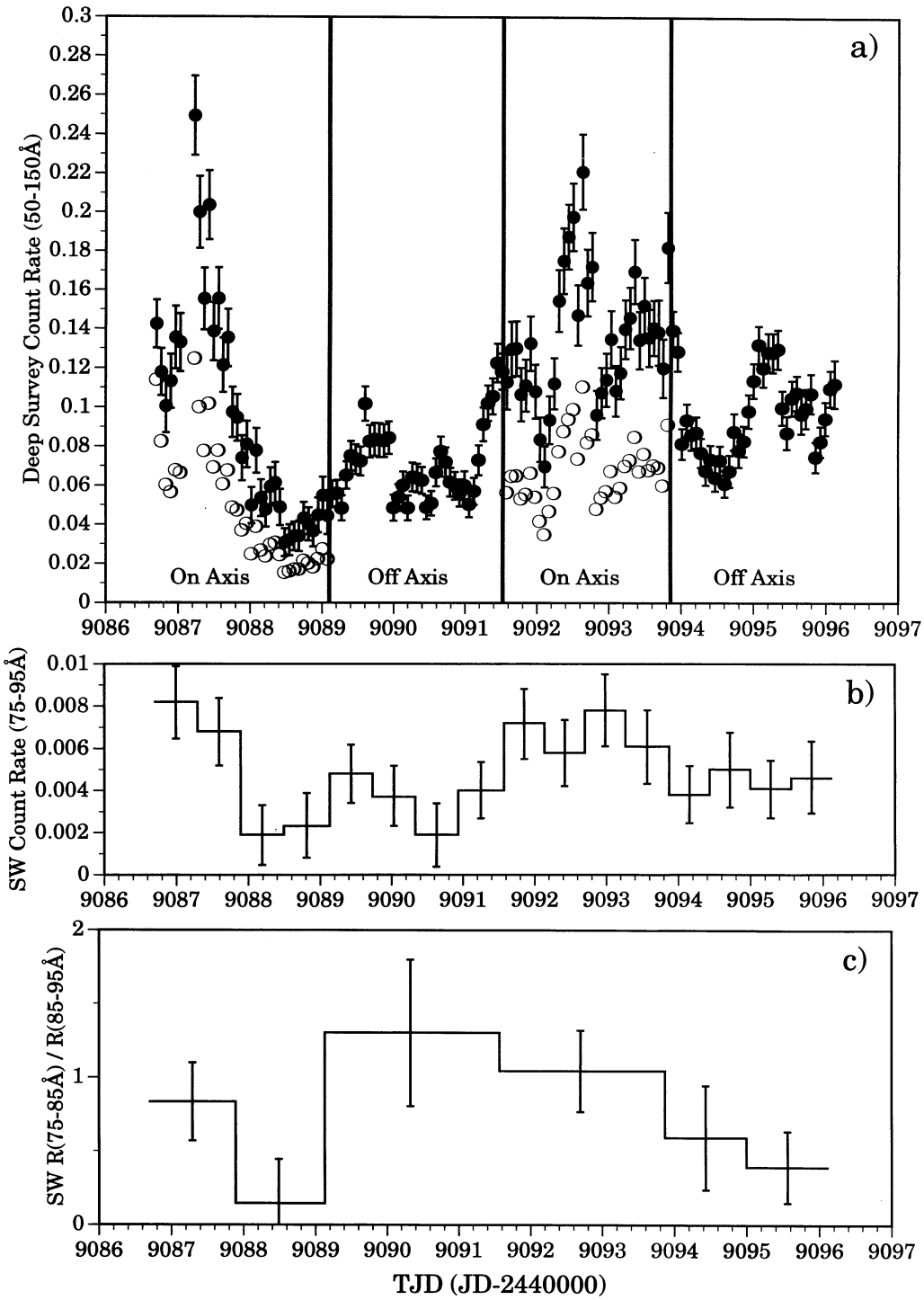

FIG. 2.—Time history of the Mrk 478 count rates and a count rate ratio. (*a*) Count rate obtained by the *EUVE* Deep Survey (DS) imaging detector. The vertical lines delineate separate pointing directions. Open circles are the original values and solid points are values corrected for the detector dead spot inefficiency as described in the text. The uncertainties are statistical only; for on-axis data, the dead spot corrections introduce a systematic uncertainty which are estimated to be 25%–50% (see Sirk 1994). (*b*) Count rate in the 75–95 Å band from the *EUVE* short-wavelength (SW) spectrometer. The rates are lower due to the smaller effective area of the spectrometer. The overall shape is consistent with the DS light curve. (*c*) A hardness ratio of the count rates in the 75–85 Å and 85–95 Å bands. The data are consistent with no color changes as the source varies. We may rule out a model where variability is caused by changes in absorption, however, because the predicted hardness *increase* can be ruled out by the data.

much poorer than for the DS detector (due to the lower effective area and higher background), so larger time bins are used. Taking a cue from the DS light curve, bins were chosen so that the first rapid drop might be discerned. Qualitatively, the SW light curve follows the DS light curve, and the hypothesis that the count rate is a constant can be ruled out at the 95% confidence level. The SW data in the first on-axis interval are consistent with a count rate drop of a factor of 3 or more, as indicated by the DS data.

3. MODELING THE EUV SPECTRUM

The source is best detected in the 83–95 Å range. At the very shortest possible wavelength, 64.5 Å, the edge of the detector shows a bright rim which makes background subtraction nearly impossible, so we begin analysis at 65 Å. There is a marginal detection of the EUV flux in the 65–70 Å range at the 2.1 σ level while the 70–75 Å band shows no evidence for a detection of the spectrum. At the long-wavelength end, the data in the 110–120 Å range give a χ^2 value of 18.7 for 10 degrees of freedom in a test against zero flux, while the 120–130 Å range gives a χ^2 of 11.0, indicating that the source spectrum is detectable only out to about 120 Å. Thus we chose the 65–120 Å wavelength range for spectral modeling. The uncertainty-weighted count rate in this range is 0.0064 ± 0.0005 count s^{-1}.

Because the spectrum shows no obvious narrow emission lines, we fitted the data to a simple power-law spectrum with absorption by neutral gas in the Galaxy and the host galaxy. We assume that this gas is not significantly ionized ($N_{\rm HeII}/N_{\rm H} = 0.01$) and that the abundance of He I is 0.09, appropriate for the interstellar medium of the Galaxy toward extragalactic sources (such as PKS 2155−304; Fruscione et al. 1993). There were three free parameters in the model: S_{90}, the flux density at 90 Å (in μJy); α, the spectral index ($S_\nu \propto \nu^{-\alpha}$), and $N_{\rm H}$. The redshift of Mrk 478, $z = 0.079$, is low enough that the effect of neutral gas in the host is virtually indistinguishable from that in the Galaxy, so $N_{\rm H} \simeq N_{\rm H,gal} + N_{\rm H,host}$. We minimized the χ^2 statistic, since the spectral uncertainties are dominated by the background subtraction and the background per 1 Å bin is greater than 100 counts (using a 10 pixel aperture in the imaging direction).

The best-fit power-law parameters are $\alpha = 27 \pm 8.5$ and $\log (N_{\rm H}) = 20.62 \pm 0.14$ (± 1 σ uncertainties for 1 degree of freedom). This value of $N_{\rm H}$ is much higher than the 21 cm value, which was measured by Lockman (1994) to be about $(1.0 \pm 0.1) \times 10^{20}$ cm^{-2}, using the method pioneered by Lockman, Jahoda, & McCammon (1986). By requiring that $N_{\rm H} = N_{\rm H,gal}$, we find $\alpha = 4.2 \pm 0.7$, $S_{90} = 85 \pm 6$ μJy, and χ^2 is 88.8 for 53 degrees of freedom. This model is plotted in Figure 1. Note that allowing for intrinsic absorption above the Galactic value only increases the fitted value of α.

The high χ^2 value indicates that the fit is not perfect: the model is formally rejected at the 99.8% confidence level. It is easy to pinpoint the main contributors to the poor χ^2 value. The points at 70 Å and 105 Å contribute 26% of the χ^2 and are likely results of unusual background fluctuations since the estimates of the net flux are both negative, which is physically impossible. Detector effects could not cause these deviations because the negative features coincidentally show up in both the on-axis and the off-axis spectra, so two different detector locations are involved. Eliminating these two points from the fit gives a model which is consistent with the data at the 90% confidence level.

We also tried fixing α to 2.3, as determined from *ROSAT* data (Gondhalekar et al. 1994), obtaining $\log (N_{\rm H}) = 19.89 \pm 0.05$ and $S_{90} = 45 \pm 4$ μJy. By contrast, a good fit to the *ROSAT* data with this same index and a slightly higher $N_{\rm H}$ gives a normalization of 109 μJy (Gondhalekar et al. 1994), indicating that Mrk 478 has dimmed by a factor of 2 or so since the *ROSAT* observations, taken 1992 January 17. The $\Delta\chi^2$ is modest, 2.1, when compared to the value from the last fit, so these two fits are practically indistinguishable.

Thermal fits did not improve the χ^2 values significantly, which is consistent with the interpretation that the bad fit is due to two points giving bad background subtractions. There is a good relation between a fitted value of a power-law index and the fitted temperature in a thermal model because the temperature is simply determined by noting the location where the power law and thermal models match spectral slopes, which is in the middle of the most significant data at about 90 Å. For the bremsstrahlung model, $kT = hc/(\lambda\alpha)$, giving $T = 3.8 \times 10^5$ K. The temperature of a blackbody model would be given by $\alpha = [hc/(kT\lambda) - 3]$, so $T = 2.2 \times 10^5$ K.

Both power-law fits were used to predict the average count rate in the DS detector, giving 0.085 count s^{-1}. Allowing the spectral index to vary within its uncertainties has no effect on the predicted count rate due to the choice of 90 Å for normalizing the spectrum. The uncertainty in the normalization is about 7%, but the systematic uncertainty in the corrections for the dead spot were previously estimated to cause a 10%–15% systematic uncertainty in the DS count rate, so the models adequately predict the DS count rate.

We attempted to determine if the spectrum hardens or softens as the source brightens by measuring the ratio of the count rates in the 75–85 Å and 85–95 Å bands during bright and dim parts of the light curve (Fig. 2*c*). Although it is difficult to tell exactly when the source is brightest due to the uncertainties in correcting the DS data for the dead spot inefficiency, it appears to be significantly brighter during the first half of the first interval and the entire third interval and dimmest during the second half of the first interval. Comparing the ratios for these sections gives a 2.3 σ difference: 0.94 ± 0.19 during the bright parts and 0.14 ± 0.30 during the dim section.

Although the count rate ratio data are marginally consistent with a simple change of the spectral normalization, we make a more stringent test of the hypothesis that the broadband variations are due to changes in the neutral column density intrinsic to the source. In this case, the source spectrum is expected to harden as it dims since the longer wavelength portion is absorbed. We have computed the expected count rate ratios for a simple power-law spectral model for a wide range of spectral indices and $\log N_{\rm H}$ in the range 19.8–20.3. For each ($\alpha - N_{\rm H}$) pair, we increased the $N_{\rm H}$ until the predicted DS count rate dropped by a factor of 3 and then determined the count rate ratio again. We found that this ratio was in the range 0.5–1.0 for $\alpha < 4$. Furthermore, the faint hardness ratio was always *higher* than the bright ratio by at least 0.3 and often 0.5. As α increases, the bright and dim hardness ratios are more similar but the bright ratios are about 2 σ too low. Thus we conclude that the spectral changes are inconsistent with variations in the neutral gas absorption local to the source.

4. DISCUSSION

4.1. *Emission-Line Models*

The spectrum clearly rules out models in which the EUV flux of Mrk 478 is dominated by emission lines. Barvainis

(1993) suggests that the EUV excess might be related to the UV component, fitting both with a bremsstrahlung spectrum with $T \approx 10^6$ K, while Turner et al. (1991) suggest that some excesses may be due to blends of iron emission lines. The *EUVE* observations can place stringent limits on both models. An optically thin plasma in coronal ionization equilibrium between 10^6 and 10^7 K will emit a number of strong lines in the 70–100 Å range. Using the MAPPINGS II code (Sutherland & Dopita 1993), we found the strongest lines in this band to be Fe IX λ82.43, 83.46, Fe X λ100.0, Fe XI λ88.00, and Fe XIII λ75.84. Optically thin plasma emission codes can be used to provide expected line fluxes as a function of temperature, which can be combined with the observations to limit the "emission measure," $n_H^2 V$, of hot plasma.

To give a concrete example, consider the Fe IX $3p^6[^1S] \rightarrow 3p^5 4d[^1P, {}^3P]$ transitions at 82.43 Å and 83.46 Å, which are expected to be strong at the temperature $T \approx 10^6$ K of peak Fe IX ionization fraction (Shull & Van Steenberg 1982; Sutherland & Dopita 1993). The line emissivity of the 83.46 Å line at temperature $(10^6 \text{ K})T_6$, normalized to n_H^2, is

$$\Lambda_{\text{FeIX}} = (1.13 \times 10^{-22} \text{ ergs cm}^3 \text{ s}^{-1}) T_6^{-1/2} f_9 \bar{\Omega}(T) \exp(-1.724/T_6), \quad (1)$$

where $\bar{\Omega} \approx 0.3$ is the Maxwellian-averaged collision strength of the transition and $f_9 \approx 0.3$ is the ionization fraction of Fe IX at peak. Here we have assumed an abundance $n_{Fe}/n_H = 4.68 \times 10^{-5}$ by number, $n_e = 1.18 n_H$, and a source distance $D = 316\, h_{75}^{-1}$ Mpc for a Hubble constant $H_0 = 75\, h_{75}$ km s^{-1} Mpc^{-1}. If the line flux is less than the (2.5 σ) limit of 10^{-4} photons cm^{-2} s^{-1}, then the optically thin emission measure is less than

$$n_H^2 V < (2.5 \times 10^{63} \text{ cm}^{-3}) T_6^{1/2} \exp(1.724/T_6) e^{\tau} f_9^{-1} \bar{\Omega}^{-1} h_{75}^{-2}, \quad (2)$$

where τ is the ISM optical depth at the observed wavelength. These lines are redshifted to 88.94 Å and 90.05 Å, where $\tau \simeq 2.6$ for $\log N_H = 20.0$. Thus, at $T = 10^6$ K, the emission measure is limited to $n_H^2 V < 2 \times 10^{66} h_{75}^{-2}$ cm^{-3}. In order to match the UV flux at 1500 Å, a bremsstrahlung emission measure of $2.7 \times 10^{69} h_{75}^{-2}$ cm^{-3} would be required. The data give a limit which is more than a factor of 10^3 below this. We conclude that bremsstrahlung emission from a thin thermal plasma can be ruled out as a model of the UV bump.

The same line of reasoning can be used to show that the EUV continuum also cannot be bremsstrahlung emission. The EUV continuum requires an even higher emission measure of 4×10^{71} cm^{-3}. The temperature is determined from the fit: $T_6 = 0.38$, at which an important emission line is Si V (80.00 Å in the rest frame or 86.3 Å in the observed frame). The predicted Si V line strength is 0.06 photons s^{-1} cm^{-2}, and the ISM optical depth at 86.3 Å is about 2.3. A line strength of 0.0001 photons s^{-1} cm^{-2} would be easily detected at 86 Å, which is a factor of 60 below the expected value. Thus we conclude that a thin thermal plasma is not a good model of the EUV continuum, either.

4.2. *An Optically Thick Thermal Model*

The *EUVE* DS data indicate substantial variability on a daily timescale or shorter, and there is also evidence of longer term variations. Folding the power-law spectral models with the *EUVE* scanner effective area gives a count rate of 0.055 count s^{-1}, which is consistent with the observed value. The *EUVE* all-sky survey measurement was obtained from TJD 9180–9187, only 85 days after the end of our spectroscopic observations (since the survey data came from a gap fill-in observation which occurred during the guest observer phase). The predicted ratio of the *EUVE* and WFC Lexan/B count rates, however, is about 2.5, but the actual rates were almost identical, indicating possible variability of a factor of 2 over the several years between the WFC and *EUVE* survey measurements.

The spectral data are consistent with a thermal origin of the emission that has high optical depth. The strong variations of the broadband EUV emission, combined with the evidence that the spectrum hardens as it brightens, can result from small changes in temperature when the bandpass is on the Wien tail. The DS count rate is very sensitive to the effective temperature because the Rayleigh-Jeans portion of the spectrum is absorbed by the Galaxy. For temperatures about 0.018 keV (the best fit), the count rate goes as $T^{8.2}$. A 10% variation of the effective temperature can cause a factor of 2 variation in the observed DS count rate. This small temperature change would go relatively unnoticed at much longer wavelengths like the UV band. In an accretion disk model, the UV and EUV bands result from different regions in the disk, so thermal variations in the inner regions may be unrelated to UV variations and so have little to do with the overall accretion rate. This effect might also explain why soft X-ray variations have a larger amplitude than UV and optical variations. The spectral softening related to the factor of 7 intensity drop (TJD 9087.3 to 9088.5) would be a change of index from 3.9 to 5.6, which is marginally detectable, consistent with the analysis in § 3.

The luminosity of the EUV component is estimated from the $\alpha = 4.7$ spectral fit to be $2.5 \times 10^{44} h_{75}^{-2}$ ergs s^{-1} in the 65–120 Å band. Due to the extremely steep spectrum, the X-ray flux from this soft component is negligible by comparison. The overall spectral energy distribution indicates that the total power per frequency decade is similar in the UV and EUV bands. If these two components were linked with a ν^{-1} power law, the total UV luminosity would then be about $1.2 \times 10^{45} h_{75}^{-2}$ ergs s^{-1}. The combination of high luminosity and short timescale variability places Mrk 478 among the most extreme of the sources studied by Elvis et al. (1991). These authors suggest that AGNs soft excesses must be optically thick, which is consistent with the overall picture developed here.

Variability of the EUV flux may be directly related to variations in the ionizing flux impinging on the broad-line clouds. Again, however, the broad lines are not observed to vary as significantly as the EUV flux, leading to an apparent contradiction. In this model, there is a natural way out: the EUV flux is isolated to a very narrow range of energies just above the blackbody peak, so that the variations in the ionizing flux are not likely to be nearly as large over the entire EUV band from 912 Å to 100 Å. Furthermore, it has been shown that many broad emission lines respond slowly to continuum changes due to the larger size of the broad line region (e.g., Peterson et al. 1991).

4.3. *Fitting an Accretion Disk Model*

We combined our EUV data with *IUE* spectra taken 1993 January 1 from Koratkar et al. (1996) and ground-based optical data taken from Edelson & Malkan (1986). Even though the optical fluxes were measured many years before, they match the UV data well at the point of overlap. The energy distribution plotted in Figure 3 has been fitted with standard models of

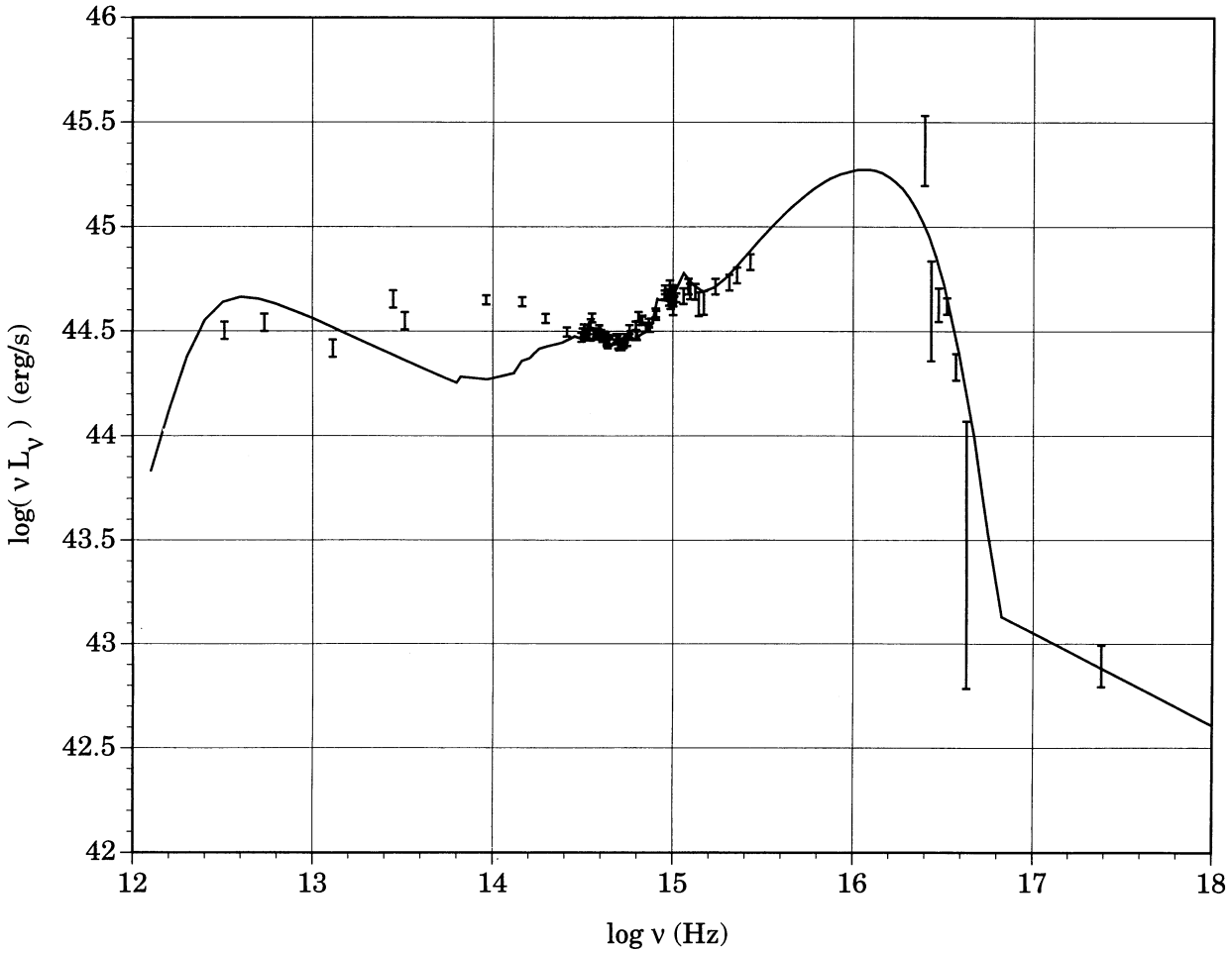

FIG. 3.—Luminosity spectrum of Mrk 478, corrected for reddening by dust and, for absorption by the Galactic interstellar gas ($N_H = 1.0 \times 10^{20}$ cm^{-2} and He/H = 0.09), assuming $H_0 = 75\,h_{75}$ km s^{-1} Mpc^{-1}. The IR and optical data are taken from Edelson & Malkan (1986), the UV data are from Koratkar et al. (1996), the hard X-ray point at 5 keV is from HEAD-A (see Remillard 1991), and the EUV data are from this paper, binned by 10 Å. Note that the observed data rise toward the UV and match the data in the EUV band well. *Solid line:* Accretion disk model fitted to the data, with added stellar light, Balmer emission, and a weak nonthermal power law. The model gives $M = 1.3 \times 10^8\,M_\odot$ and $\dot{M} = 0.3\,h_{75}^{-2}\,M_\odot$ yr^{-1} for an assumed inclination of cos $i = 0.5$.

optically thick, geometrically thin accretion disks, as in Malkan (1983) and Sun & Malkan (1989). For an assumed inclination of cos $i = 0.5$, we find $M = 1.3 \times 10^8\,M_\odot$ and $\dot{M} = 0.3\,h_{75}^{-2}\,M_\odot$ yr^{-1}. Small amounts of galaxy luminosity and Balmer continuum emission improved the fit in the optical band. The fits in the IR are poor, but this component may be due to heated dust. The fit in this region has little effect on the accretion disk parameters.

The best-fit parameters change with cos i, which cannot be determined from these data. As Sun & Malkan (1989) pointed out, for a rapidly spinning black hole the best-fitting mass accretion rate is essentially independent of inclination angle, while the best-fitting black hole mass doubles for every decrease of 0.25 in cos i. Correspondingly, $L/L_{\rm Edd}$ increases with cos i because $\dot{M}$ stays approximately constant (given by the total luminosity) while the peak effective temperature of the disk decreases with cos i. However, if one requires sub-Eddington accretion, then cos $i < 0.75$ is required; the disk must be highly inclined to the line of sight. In the best fit, the highest temperature reached in the inner disk is 300,000 K, generating substantial EUV radiation, some of which is Doppler-boosted up to the soft X-rays to match the observed flux levels. At this high temperature, our assumption that the local flux is emitted in a pure blackbody spectrum would be justified only if the viscosity in the disk is relatively low, so that the density and optical depth to true absorption are relatively high. Given that the EUV/soft X-ray excess in Mrk 478 is probably unusually strong, it is not unreasonable to invoke a somewhat favorable viewing inclination to explain it.

We wish to thank the *EUVE* Guest Observer Center Team, in particular Jean Dupuis and Alexandria Weircigroch, for their advice and support during the initial analysis. We are indebted to F. Jay Lockman for providing an accurate value of the H I column density to this source, to David Koo for providing an optical spectrum of $M_\odot$ at Lick during the time of the *EUVE* observations, and to Ralph Sutherland for discussions of plasma emission codes. This work has been supported by NASA contract NAS5-32485 to Eureka Scientific, Inc., a private corporation created to promote the active pursuit of scientific research, and in part by a NASA *IUE* grant NAG5-2189.

REFERENCES

Barvainis, R. 1993, ApJ, 412, 513
Branduardi-Raymont, G., et al. 1985, MNRAS, 216, 1043
Edelson, R. A., & Malkan, M. A. 1986, ApJ, 308, 59
Elvis, M., Giommi, P., Wilkes, B. J., & McDowell, J. 1991, ApJ, 378, 537
Elvis, M., Lockman, F. J., & Wilkes, B. J. 1989, AJ, 97, 777
Fruscione, A., Bowyer, S., Königl, A., & Kahn, S. 1993, ApJ, 422, L55
Gondhalekar, P. M., Kellett, B. J., Pounds K. A., Matthews, L., & Quenby, J. J. 1994, MNRAS, 268, 973
Koratkar, A., Marshall, H. L., Madejski, G. M., Porter, A., & Urry, C. M. 1996, in preparation
Lockman, F. J. 1994, private communication
Lockman, F. J., Jahoda, K., & McCammon, D. 1986, ApJ, 302, 432
Malina, R. F., et al. 1994, AJ, 107, 751
Malkan, M. A. 1983, ApJ, 268, 582
Marr, G., & West, J. 1976, At. Data Nucl. Data Tables, 18, 497
Marshall, H. L. 1991, in EUV Astronomy, ed. R. F. Malina & C. S. Bowyer (New York: Pergamon), 228
Marshall, H. L. 1995 ApJ, submitted
Marshall, H. L., & Dupuis, 1995, in preparation
Marshall, H. L., Fruscione, A., & Carone, T. E. 1995, ApJ, 429, 90
Peterson, B. M., et al. 1991, ApJ, 368, 119
Pounds, K., et al. 1993, MNRAS, 260, 77
Remillard, R. 1991, unpublished MC-LASS catalog
Shull, J. M., & Van Steenberg, M. E. 1982, ApJS, 48, 95
Sirk, M. 1994, internal *EUVE* memo MMS/EUVE/0084/94
Stark, A. A., Gammie, C. F., Wilson, R. W., Bally, J., Linke, R. A., Heiles, C., & Hurwitz, M. 1992, ApJS, 79, 77
Sun, H-S., & Malkan, M. A. 1989, ApJ, 346, 68
Sutherland, R. S., & Dopita, M. A. 1993, ApJS, 88, 253
Turner, T. J., & Pounds, K. A. 1989, MNRAS, 240, 833
Turner, T. J., Weaver, K. A., Mushotzky, R. F., Holt, S. S., & Madejski, G. M. 1991, ApJ, 381, 85
Wilkes, B. J., & Elvis, M. 1987, ApJ, 323, 243